



# Inefficient development of syncytiotrophoblasts in the *Atp11a*-deficient mouse placenta

Yuki Ochiai<sup>a</sup>, Chigure Suzuki<sup>b,c</sup>, Katsumori Segawa<sup>a,1</sup>, Yasuo Uchiyama<sup>b,c</sup>, and Shigekazu Nagata<sup>a,d,2</sup>

Contributed by Shigekazu Nagata; received January 12, 2022; accepted March 22, 2022; reviewed by Raymond Birge and Yasushi Hirota

The P4-ATPases ATP11A and ATP11C function as flippases at the plasma membrane to translocate phosphatidylserine from the outer to the inner leaflet. We herein demonstrated that *Atp11a*-deficient mouse embryos died at approximately E14.5 with thin-walled heart ventricles. However, the cardiomyocyte- or epiblast-specific *Atp11a* deletion did not affect mouse development or mortality. ATP11C may have compensated for the function of ATP11A in most of the cell types in the embryo. On the other hand, *Atp11a*, but not *Atp11c*, was expressed in the mouse placenta, and the *Atp11a*-null mutation caused poor development of the labyrinthine layer with an increased number of TUNEL-positive foci. Immunohistochemistry and electron microscopy revealed a disorganized labyrinthine layer with unfused trophoblasts in the *Atp11a*-null placenta. Human placenta-derived choriocarcinoma BeWo cells expressed the *ATP11A* and *ATP11C* genes. A lack of ATP11A and ATP11C eliminated the ability of BeWo cells to flip phosphatidylserine and fuse when treated with forskolin. These results indicate that flippases at the plasma membrane play an important role in the formation of syncytiotrophoblasts in placental development.

flippase | phosphatidylserine | cell fusion | placenta | trophoblast

Plasma membranes in eukaryotes comprise a lipid bilayer in which phosphatidylserine (PtdSer) is exclusively confined to the inner leaflet (1, 2). PtdSer is reversibly or irreversibly exposed on the cell surface and serves as a signal or scaffold for enzymes in various biological processes (3–5). PtdSer irreversibly exposed on the surface of apoptotic cells serves as an “eat me” signal, that on activated platelets binds to blood clotting factors and enhances their protease activities, and that exposed on tumor cells or in their environment suppresses the immune system (3).

ATP11A and ATP11C, members of the P4-type Adenosine triphosphatase (ATPase) family (6, 7), are membrane proteins that carry 10 transmembrane regions and a cytoplasmic ATPase domain (8–10). They are localized to the plasma membrane with a CDC50A chaperone and function as flippases that translocate PtdSer and phosphatidylethanolamine from the outer to inner leaflet. When PtdSer is exposed to the cell surface, these two flippases at the plasma membrane are inactivated by a high concentration of Ca<sup>2+</sup> or caspase-mediated cleavage (8, 9). To conform to the rapid exposure of PtdSer on apoptotic cells and activated platelets, another enzyme called scramblase is activated and nonspecifically scrambles phospholipids between the outer and inner leaflets (5).

Although ATP11A and ATP11C are ubiquitously expressed in various cells with a redundant function, a loss-of-function mutation in *Atp11c* in humans and mice causes multiple phenotypes. *Atp11c*<sup>y1-</sup> mice developed B cell lymphopenia, cholestasis, and mild anemia (11–14), while a human patient defective in *ATP11C* exhibited hemolytic anemia (15). We previously reported that mouse B cell precursors did not express *Atp11a* at the pre-B cell stage (16). Therefore, *Atp11c*-deficient pre-B cells do not have flippases, expose PtdSer, and are engulfed alive by surrounding macrophages in bone marrow, which leads to B cell lymphopenia.

In the present study, we demonstrated that *Atp11a*-deficient mice were embryonic lethal or died at approximately embryonal day (E) 14.5 with improper heart development and anemia. Nevertheless, the cardiomyocyte- or epiblast-specific deletion of *Atp11a* did not adversely affect mouse development. We found that the mouse placenta, particularly trophoblasts in the labyrinthine placental layer, expressed ATP11A but not ATP11C flippase. The labyrinth is a porous location in the placenta at which nutrients, oxygen, and waste are exchanged between maternal and fetal blood (17). Two tightly adhered layers of syncytiotrophoblasts (SynT-I and SynT-II), generated by the fusion of trophoblasts, separate the maternal and fetal blood compartments in the mouse labyrinth (18). Syncytiotrophoblasts in the *Atp11a*-deficient placenta were not well developed, possibly due to inefficient cell fusion. Accordingly, the deletion of the *ATP11A* and *ATP11C* genes strongly reduced the ability of the human BeWo

## Significance

Plasma membranes are composed of a lipid bilayer in which phosphatidylserine (PtdSer) is confined to the inner leaflet by the action of flippase that translocates PtdSer from the outer to inner leaflets. Two P4-ATPases (ATP11A and ATP11C) work as flippase at plasma membranes. Here, we report that the mouse placenta expresses only ATP11A, and *Atp11a*-deficient mouse embryos die during embryogenesis due to inefficient formation of syncytiotrophoblasts in the placental labyrinth. The flippase-null mutation inactivates human choriocarcinoma BeWo cells to translocate PtdSer into the inner leaflet and undergo cell fusion. These findings highlight the importance of flippase to regulate the distribution of phospholipids for cell fusion, at least in trophoblast fusion.

Author contributions: Y.O., K.S., and S.N. designed research; Y.O. and C.S. performed research; Y.O., C.S., K.S., Y.U., and S.N. analyzed data; and Y.O., K.S., and S.N. wrote the paper.

Reviewers: R.B., Rutgers The State University of New Jersey; and Y.H., Tokyo Daigaku.

The authors declare no competing interest.

Copyright © 2022 the Author(s). Published by PNAS. This open access article is distributed under Creative Commons Attribution-NonCommercial-NoDerivatives License 4.0 (CC BY-NC-ND).

<sup>1</sup>Present address: Department of Medical Chemistry, Medical Research Institute, Tokyo Medical and Dental University, Tokyo 113-8510, Japan.

<sup>2</sup>To whom correspondence may be addressed. Email: snagata@ifrec.osaka-u.ac.jp.

This article contains supporting information online at <http://www.pnas.org/lookup/suppl/doi:10.1073/pnas.2200582119/-DCSupplemental>.

Published April 27, 2022.

choriocarcinoma cell line to fuse in response to forskolin. These results indicate that the flipping of PtdSer into the plasma membrane inner leaflet is necessary for efficient cell fusion to establish syncytiotrophoblasts.

## Results

### Developmental Defects and Embryonic Lethality in *Atp11a*<sup>komp/komp</sup> Mice.

*Atp11a*<sup>+/<sup>komp</sup></sup> mice harbor the knockout-first allele in the *Atp11a* gene (SI Appendix, Fig. S1). *Atp11a*<sup>+/<sup>komp</sup></sup> mice grew normally and had no abnormalities. When they were intercrossed, no *Atp11a*<sup>komp/komp</sup> (*Atp11a*<sup>kl/kl</sup>) mice were found among 107 offspring at the age of 4 wk (Fig. 1A). A genotype analysis of embryos indicated that *Atp11a*<sup>kl/kl</sup> mice survived according to Mendelian law until E13.5 but started to die thereafter (Fig. 1A). The surviving E13.5 *Atp11a*<sup>kl/kl</sup> embryos were significantly smaller (by ~10%) than littermate *Atp11a*<sup>+/<sup>komp</sup></sup> or *Atp11a*<sup>+/<sup>+</sup></sup> embryos and showed anemia (Fig. 1B).

The *Atp11a*<sup>komp</sup> allele carries the *LacZ* gene in intron 6 of the *Atp11a* gene (SI Appendix, Fig. S1). When E13.5 *Atp11a*<sup>kl/kl</sup> embryos were subjected to the in situ 5-bromo-4-chloro-3-indolyl-β-D-galactoside (X-gal) staining of whole-mount embryos, intense staining was observed in the choroid plexus, heart, dorsal root ganglion, mesentery, and tongue (Fig. 1C). Strong β-galactosidase (βGal) activity was detected in the ventricles and atrium regions. Cells in the E13.5 heart were dissected and stained for βGal activity using the spirobased immobilisable diethylrhodol-βGal (SPiDER) technique (19). As shown in Fig. 1D, cardiac troponin T (cTnT)-positive cardiac myocytes showed positive signals, indicating that the *Atp11a* gene was explicitly expressed in cardiac myocytes.

A histological analysis showed a defect at the ventricular septum of the heart from the E13.5 *Atp11a*<sup>kl/kl</sup> embryo (Fig. 1E). In addition, the heart myocardium of E13.5 mutant mice was thinner than that of the littermates due to a reduced number of myocardium layers at the ventricular apex (Fig. 1F). These results suggested that developmental disorders in *Atp11a*<sup>kl/kl</sup> mice were caused by the lack of ATP11A in cardiac myocytes. Therefore, we generated the *Atp11a* allele flanked by loxP (*Atp11a*<sup>fllox/fllox</sup> mice) (SI Appendix, Fig. S1) and crossed these mice with mice carrying the *Cre* gene under the promoter of the α-Myosin heavy-chain gene (*αMhc-Cre*) that specifically expresses *Cre* in cardiac myocytes (20). Surprisingly, the *Atp11a*<sup>fllox/fllox</sup> mice carrying *αMhc-Cre* were born and developed normally (Fig. 1G). Genotyping with DNA from the heart indicated that the *Atp11a* allele was mutated as expected and designated as *Atp11a*<sup>Δ/Δ</sup>. These results showed that abnormal cardiac development in *Atp11a*<sup>kl/kl</sup> mice was not due to the *Atp11a* deficiency in cardiac myocytes. We previously reported that among 14 members of the P4-ATPase family, ATP11A and ATP11C localized to the plasma membrane were ubiquitously expressed and exhibited redundant activity (8). A real-time RT-PCR analysis indicated that *Atp11c* messenger ribonucleic acid (mRNA) was present at ~30% of *Atp11a* mRNA in the heart (Fig. 1H), suggesting that flippase activity provided by ATP11C was sufficient to maintain homeostasis in the heart.

### Lethal Effect of the Abnormal Placenta in *Atp11a*-Null Mice.

Perez-Garcia et al. (21) reported that among embryonic lethal knockout mice, 35% of those dying by E9.5 to E14.5 had placental abnormalities, which were often accompanied by the abnormal development of the heart or brain (21–23). We attributed the lethality of *Atp11a*-deficient mice to a defect in the placenta. Western blotting with a monoclonal antibody (mAb; clone 4-C11) against mouse ATP11A showed an ~130-kDa

band in the wild-type heart but not in the *Atp11a*<sup>kl/kl</sup> heart (Fig. 2A), which confirmed the specificity of the mAb. The intensity of 130-kDa ATP11A in lysates from the wild-type mouse placenta was approximately 10-fold stronger than in those from the heart. A markedly reduced but still significant level of the ATP11A band was observed in the *Atp11a*<sup>kl/kl</sup> placenta, potentially from maternal (*Atp11a*<sup>+/<sup>komp</sup></sup>)-derived decidual cells. A real-time RT-PCR analysis indicated that the level of *Atp11a* mRNA normalized to that of *glyceraldehyde-3-phosphate dehydrogenase* (*Gapdh*) mRNA was more than 10-fold higher in the placenta (Fig. 2B) than in the heart (Fig. 1H). In contrast, *Atp11c* mRNA expression was negligible in the E13.5 placenta (Fig. 2B). X-gal staining of the whole placenta revealed that cells in the labyrinthine layer, but not in the spongiotrophoblast layer, expressed the βGal gene under the *Atp11a* gene promoter (Fig. 2C).

We then deleted the *Atp11a* gene in an epiblast-specific manner by crossing *Atp11a*<sup>fllox/fllox</sup> mice with *Sex determining region Y-box 2* (*Sox2*)-*Cre* transgenic mice that expressed *Cre* in epiblasts (24–26). As shown in Fig. 2D, *Atp11a*-deficient mice with the *Sox2-Cre*<sup>+</sup>*Atp11a*<sup>Δ/Δ</sup> genotype were born at a lower number than expected (Fig. 2D) but grew normally. A Western blot analysis indicated that the ATP11A protein was not present in the heart, kidneys, or lungs of *Sox2-Cre*<sup>+</sup>*Atp11a*<sup>Δ/Δ</sup> mice (Fig. 2E). Histological analysis of the heart from the mice at 16 mo of age showed no apparent abnormality (SI Appendix, Fig. S2). These results showed that ATP11A was dispensable for mouse embryos and adulthood but was indispensable for placental development.

### Abnormal Labyrinthine Layer in the *Atp11a*-Null Placenta.

When *Atp11a*<sup>+/<sup>komp</sup></sup> mice were intercrossed, the E13.5 placentas of *Atp11a*<sup>kl/kl</sup> embryos were smaller and thinner than those of their littermates of the *Atp11a*<sup>+/<sup>+</sup></sup> or *Atp11a*<sup>+/<sup>komp</sup></sup> genotype (Fig. 3A). The weight of placentas was ~70% of those for the control littermates. The mouse placenta comprises the maternal decidua and fetal parts that consist of the spongiotrophoblast and labyrinthine cell layers and chorion (Fig. 3B). A histological analysis of the placenta in E13.5 *Atp11a*<sup>kl/kl</sup> mice showed that their labyrinthine layer was 30% thinner than that in *Atp11a*<sup>+/<sup>+</sup></sup> mice (Fig. 3D). In contrast, the size of the spongiotrophoblast layer was similar to that of the control littermates.

A close examination of the wild-type labyrinth showed juxtaposed maternal blood lacunae and fetal blood vessels separated by syncytial and mononuclear trophoblastic cell layers (Fig. 3C). Fetal blood vessels lined by endothelial cells contained primitive nucleated erythrocytes that were easily distinguished from maternal sinusoids carrying enucleated erythrocytes. In comparison with the wild-type placenta labyrinth, the *Atp11a*<sup>kl/kl</sup> placenta labyrinth was less packed and only a few fetal blood vessels containing nucleated erythrocytes were present (Fig. 3C). Maternal sinusoids were also not surrounded well by syncytiotrophoblasts. A similar abnormality was observed in the labyrinth of E11.5 *Atp11a*<sup>kl/kl</sup> placenta (SI Appendix, Fig. S3).

### Abnormal Syncytiotrophoblasts in the Labyrinthine Layer of the *Atp11a*-Null Placenta.

In the mouse placenta, the SynT-I and SynT-II layers surrounded maternal sinusoids in the labyrinthine layer (Fig. 4A). Immunostaining with anti-monocarboxylate transporter (MCT)1 and anti-MCT4, which are explicitly expressed in SynT-I and SynT-II, respectively (27), showed that SynT-I and SynT-II were closely associated in the wild-type placental labyrinth. On the other hand, the cell layers expressing MCT1 or MCT4 were not well connected

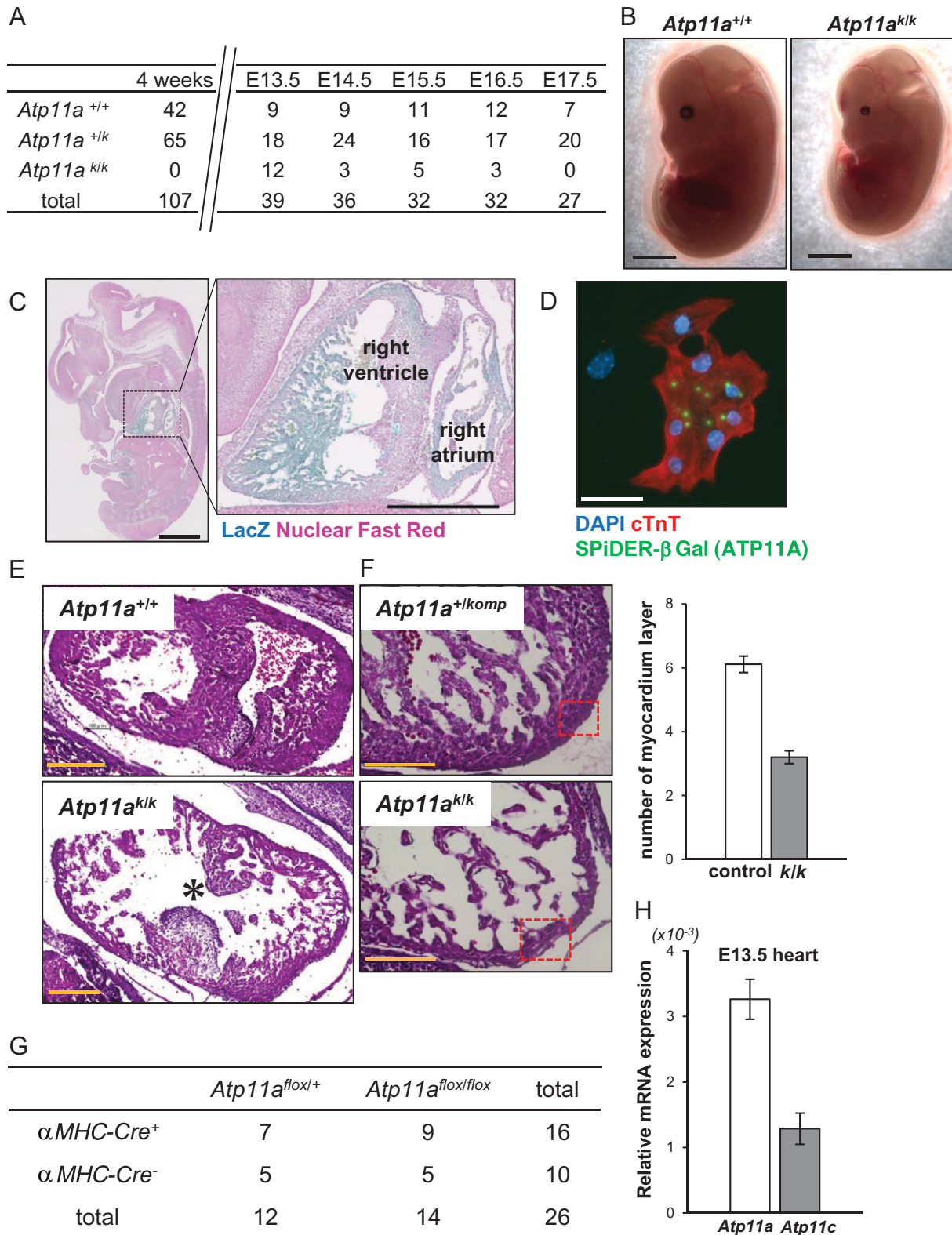


**Fig. 1.** Developmental heart defect in *Atp11a*-null embryos. (A) *Atp11a*<sup>+/*komp*</sup> mice were intercrossed, and the genotype of littermates at the age of 4 wk or the indicated embryonal day was identified. (B) The appearance of E13.5 *Atp11a*<sup>+/+</sup> and *Atp11a*<sup>*k/k*</sup> littermate embryos. *Atp11a*<sup>*k/k*</sup> embryos were smaller and paler than wild-type embryos. Scale bar, 2 mm. (C) E13.5 *Atp11a*<sup>*k/k*</sup> embryos were stained with X-gal (blue) and counterstained with nuclear fast red (pink). Scale bar, 1 mm. *Right*: Enlarged area of the dotted box. Scale bar, 500  $\mu$ m. (D) Cardiomyocytes prepared from E13.5 *Atp11a*<sup>+/*komp*</sup> hearts were stained with SPiDER- $\beta$ Gal (green), anti-cTnT Ab (red), and DAPI (blue). Scale bar, 50  $\mu$ m. (E and F) Sections of E13.5 *Atp11a*<sup>+/+</sup> or *Atp11a*<sup>+/*komp*</sup> and *Atp11a*<sup>*k/k*</sup> littermate embryos were stained with H&E. The ventricular septum (E) and right ventricular apex (F) are shown. Scale bar, 200  $\mu$ m (E), 100  $\mu$ m (F). The asterisk in E points to the ventricular septal defect in the *Atp11a*<sup>*k/k*</sup> embryo. The myocardial layer is thinner in *Atp11a*<sup>*k/k*</sup> embryos (F). The number of myocardial layers in the boxed area was quantified for four to six sections per mouse ( $n = 3$ ), and the average values were plotted with SD (bar) on the *Right*. (G) *Atp11a*<sup>*fllox/fllox*</sup> and  $\alpha$ .MHC-Cre<sup>+</sup>-*Atp11a*<sup>*fllox/+*</sup> mice were crossed, and the genotype of obtained pups at the age of 4 wk was identified. The number of mice with the indicated genotype is shown. (H) mRNAs for the *Atp11a* and *Atp11c* genes in E13.5 wild-type mouse fetal hearts ( $n = 3$ ) were quantified by real-time RT-PCR, and their relative levels against *Gapdh* mRNA were plotted with SD (bar).

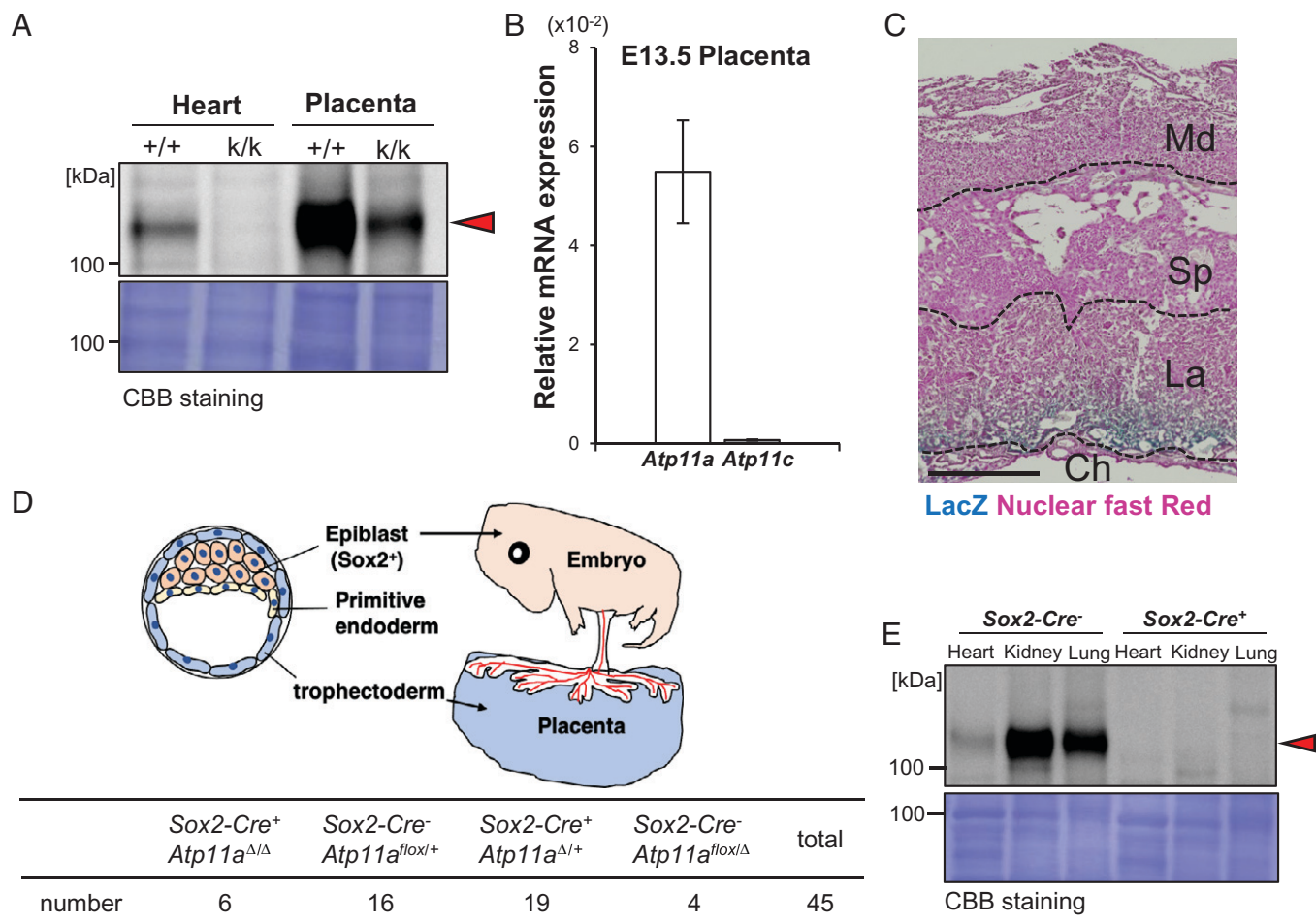


**Fig. 2.** Normal development of epiblast-specific *Atp11a*-deficient mice. (A) Tissue homogenates (8.5  $\mu$ g of protein) from the heart and placenta of E13.5 wild-type (+/+) and *Atp11a<sup>k/k</sup>* (k/k) embryos were separated by 7.5% SDS-PAGE, transferred to a PVDF membrane, and analyzed by Western blotting with anti-ATP11A mAb. The molecular mass of standard proteins is shown in kilodaltons. The red arrowhead shows ATP11A. *Bottom*: Membrane was stained with Coomassie Brilliant Blue (CBB). (B) mRNAs for *Atp11a* and *Atp11c* in the E13.5 wild-type mouse placenta ( $n = 3$ ) were quantified by real-time RT-PCR, and their relative levels against *Gapdh* mRNA were plotted with SD (bars). (C) Male *Atp11a<sup>+/-komp</sup>* mice were crossed with wild-type female mice. On day 13 of pregnancy, the placenta was dissected and stained by X-gal (blue) and nuclear fast red (pink). Md, maternal decidua; Sp, spongiotrophoblast layer; La, labyrinthine layer; Ch, chorion. Scale bar, 500  $\mu$ m. (D) *Sox2-Cre<sup>+</sup>Atp11a<sup>Δ/+</sup>* mice were crossed with *Atp11a<sup>fllox/fllox</sup>* mice, and the genotypes of 45 pups at the age of 4 wk were identified. The number of mice carrying the indicated genotype is shown. *Upper*: Schematic for blastocyst development. The blastocysts consist of epiblasts, primitive endoderm, and trophoctoderm. Epiblasts differentiate into the embryo, the primitive endoderm into the yolk sac, and the trophoctoderm into the placenta. (E) Tissue lysates (6  $\mu$ g of protein) from the heart, kidney, and lung of *Atp11a<sup>fllox/fllox</sup>* and *Atp11a<sup>Δ/Δ</sup>* mice at the age of 9 to 16 wk were separated by 7.5% SDS-PAGE and analyzed by Western blotting with anti-ATP11A mAb. The molecular mass of the standard proteins is shown in kilodaltons. The red arrowhead shows the band ATP11A. *Lower*: Membrane stained with CBB.

in the *Atp11a<sup>k/k</sup>* placenta (Fig. 4B), suggesting that syncytiotrophoblasts were not appropriately developed in the *Atp11a<sup>k/k</sup>* placenta.

To further characterize the defect in the *Atp11a<sup>k/k</sup>* placenta, we observed the E13.5 placenta under a transmission electron microscope. As shown in Fig. 4C, the wild-type labyrinth showed the layer of mononuclear sinusoidal trophoblast giant cells, the SynT-I cell layer, and the vacuole-containing SynT-II cell layer (17, 28). On the other hand, although endothelial cells and vacuole-containing cells were identified in the labyrinth of the *Atp11a<sup>k/k</sup>* placenta, the SynT-I and SynT-II layers were poorly organized (Fig. 4C). Scanning electron micrography of the wild-type labyrinthine layer from the maternal blood side showed giant cells that were expected to be syncytiotrophoblasts (Fig. 4D). On the other hand, the majority of cells were small in the *Atp11a<sup>k/k</sup>* labyrinth, while few giant cells were present, suggesting the inefficient fusion of trophoblasts. Transmission electron microscopy showed many trophoblasts carrying degenerated nuclei in the *Atp11a<sup>k/k</sup>* labyrinth (Fig. 4C). Accordingly, the number of terminal deoxynucleotidyl

transferase dUTP nick end labeling (TUNEL)-positive cells in the *Atp11a<sup>k/k</sup>* placental labyrinthine layer was about fivefold higher than in the *Atp11a<sup>+/+</sup>* placental labyrinthine layer (Fig. 4E). In addition, a real-time RT-PCR analysis showed that the mRNA levels of *Mct1*, transferrin receptor protein (*Tfrc*), *Mct4*, and chorion-specific transcription factor (*Gcm1*) genes, which are expressed in syncytiotrophoblasts (29, 30), were lower in the E13.5 *Atp11a<sup>k/k</sup>* placenta than in the wild-type placenta (Fig. 4F). These results suggested that *Atp11a*-deficient trophoblasts incapable of forming syncytiotrophoblasts died.

**Inefficient Cell Fusion of *ATP11A<sup>-/-</sup>ATP11C<sup>-/-</sup>* BeWo Cells.** To examine the effects of flippase on the formation of syncytiotrophoblasts, we investigated human BeWo cells, which undergo cell fusion into syncytiotrophoblast-like cells when treated with forskolin (31). Real-time RT-PCR showed that BeWo cells expressed the *ATP11A* and *ATP11C* genes (Fig. 5A), and the expression level of *ATP11A* mRNA increased following the treatment with 20  $\mu$ M forskolin for 48 h. We established *ATP11A<sup>-/-</sup>ATP11C<sup>-/-</sup>* (DKO) BeWo cells by the CRISPR-

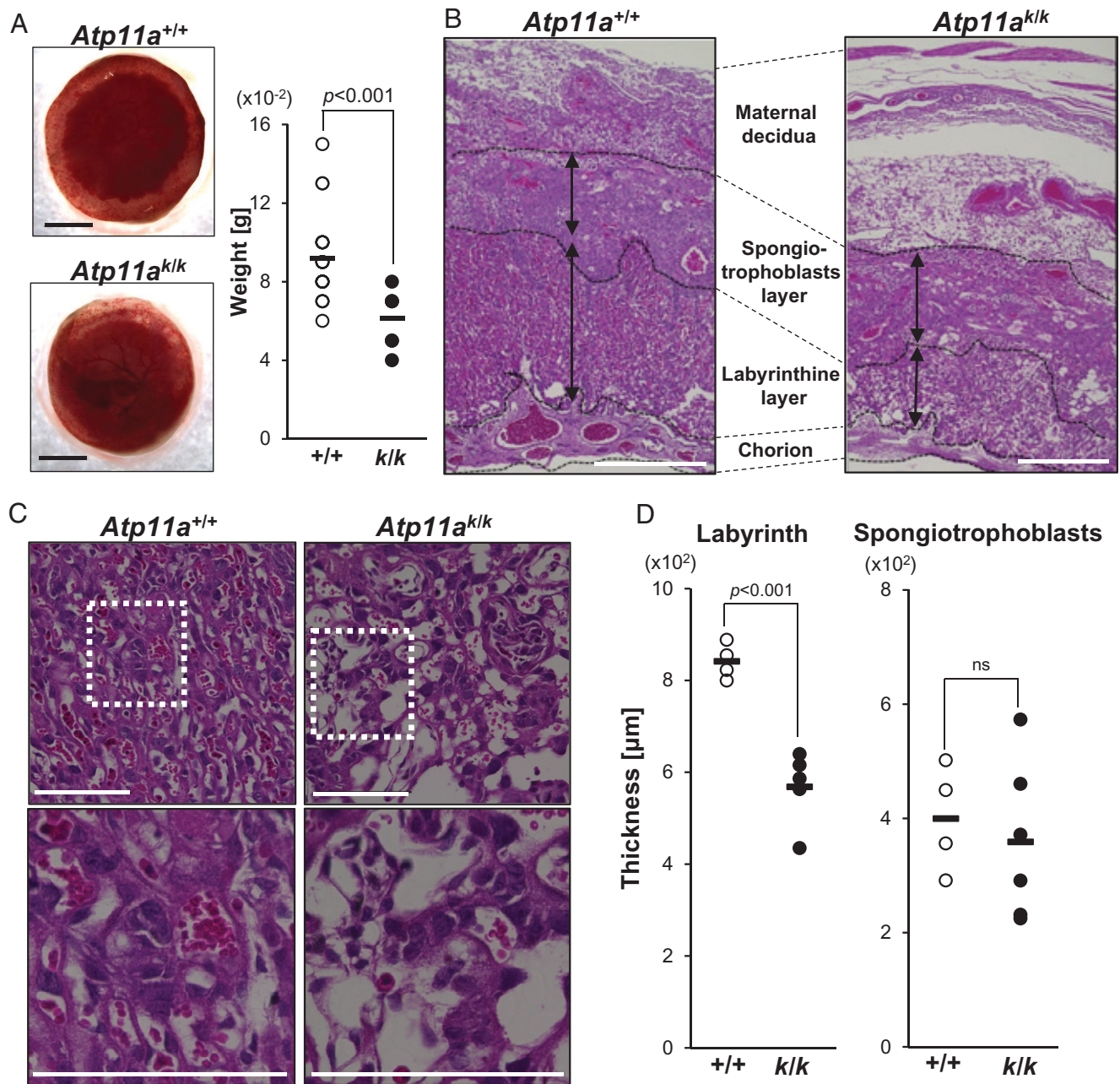


**Fig. 3.** The abnormal labyrinthine layer of the *Atp11a*-deficient placenta. *Atp11a*<sup>+/*klomp*</sup> mice were intercrossed, and placentas were removed at E13.5 and genotyped. (A) *Left*: Representative appearance of the *Atp11a*<sup>+/+</sup> (+/+) and *Atp11a*<sup>klk</sup> (k/k) placenta. Scale bar, 1 mm. *Right*: Weights of the placentas from control (*Atp11a*<sup>+/+</sup> or *Atp11a*<sup>+/*klomp*</sup>) (*n* = 22) and *Atp11a*<sup>klk</sup> (*n* = 7) mice were plotted with the average (bars). *P* values were calculated by Student's *t* test. (B and C) Histological analysis of the placenta (B) and labyrinthine layer (C). Paraffin sections from the *Atp11a*<sup>+/+</sup> or *Atp11a*<sup>klk</sup> placenta were stained with H&E and observed by microscopy. *Bottom*: Higher-magnification images of the boxed regions. Scale bar, 500 μm (B), 200 μm (C). (D) The lengths of the Sp and La in the center of the placenta indicated by black arrows in B were measured in three sections per placenta dissected from different pregnant mice (*n* = 4 for *Atp11a*<sup>+/+</sup> and *n* = 6 for *Atp11a*<sup>klk</sup>). The thickness of each placenta was plotted with the average value (bars). *P* values were calculated by Student's *t* test. ns, not significant.

Cas9 system (32) (SI Appendix, Fig. S4). As shown in Fig. 5B, wild-type BeWo cells incorporated nitrobenzoxadiazole (NBD)-labeled PtdSer (NBD-PS); however, this activity was completely lost in *DKO*-BeWo cells. The transformation of *DKO*-BeWo with human ATP11A rescued *DKO*-BeWo to flip or translocate NBD-PS into cells. To further confirm the contribution of ATP11A to the establishment of an asymmetrical distribution of PtdSer, cells were treated with 5 μM ionomycin, a Ca<sup>2+</sup> ionophore, to activate Ca<sup>2+</sup>-dependent scramblases, such as TMEM16F (33). This treatment resulted in the exposure of PtdSer in most populations of wild-type, *DKO*, and *DKO*-ATP11A BeWo cells (Fig. 5C). When the ionomycin was

removed, PtdSer on the surface of wild-type BeWo cells gradually disappeared at 25 °C, indicating that PtdSer was translocated into the inner leaflet of the plasma membrane. This internalization of PtdSer was severely retarded in *DKO*-BeWo cells, and more than 80% of the cell population continued to expose PtdSer after a 30-min incubation. On the other hand, *DKO*-expressing ATP11A regained the ability to internalize PtdSer. These results indicated that ATP11A and ATP11C flippases at the plasma membrane were essential for rapidly establishing the asymmetrical distribution of PtdSer, similar to mouse WR19L lymphoma cells (16).

Wild-type, *DKO*, and *DKO*-ATP11A BeWo cells at ~10% confluency were then treated for 48 h with 20 μM forskolin or

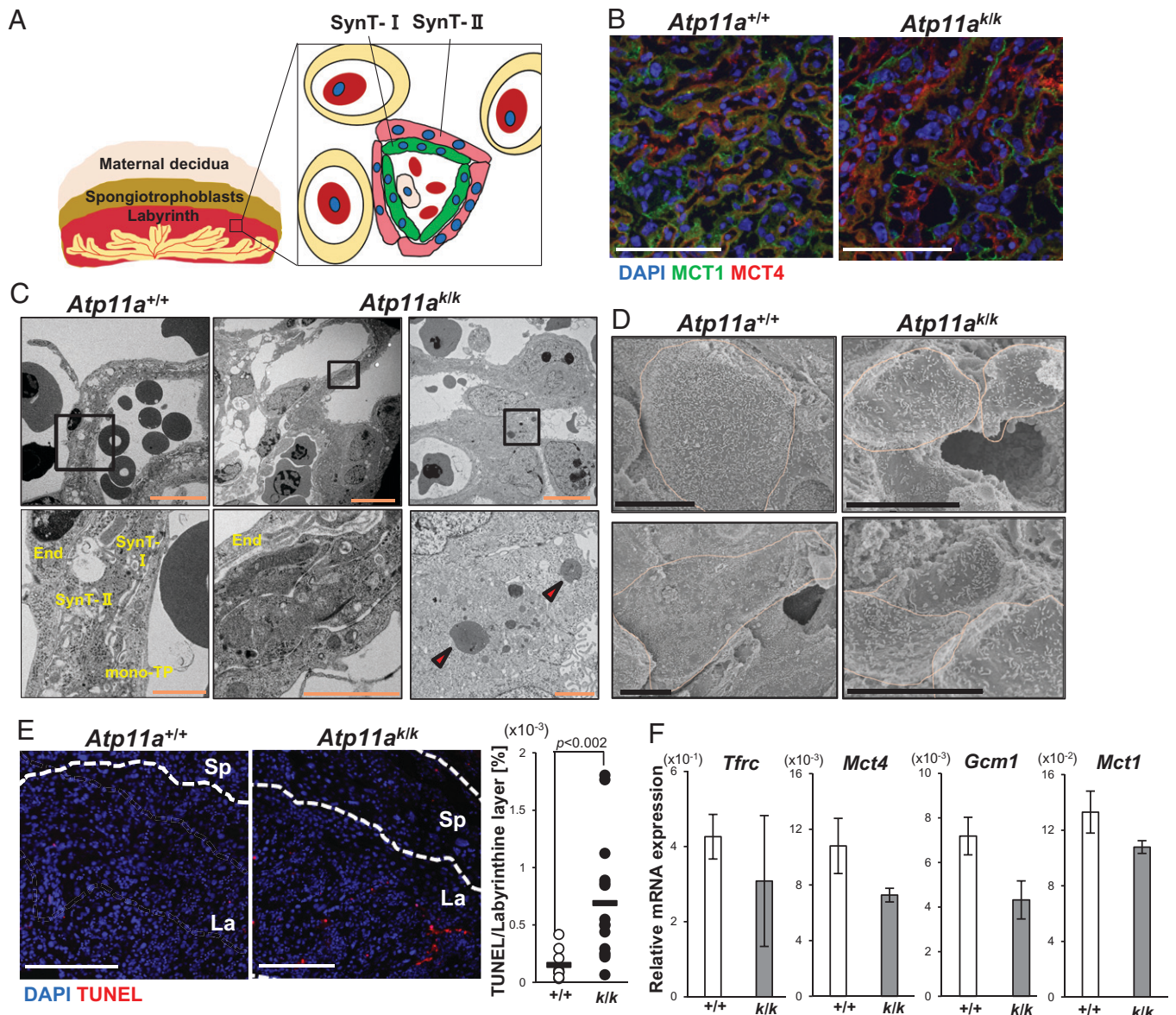


**Fig. 4.** Abnormal syncytiotrophoblasts in the *Atp11a*-deficient placenta. (A) A schematic representation of syncytiotrophoblasts in the mouse placental labyrinthine layer. Two layers of syncytiotrophoblasts, SynT-I (green) and SynT-II (pink), separate fetal and maternal blood. SynT-I and SynT-II express MCT1 and MCT4, respectively. Nuclei are shown in the blue circle. Red blood cells are in red. (B) Cryosections of the E13.5 *Atp11a<sup>+/+</sup>* and *Atp11a<sup>klk</sup>* placenta were stained with anti-MCT1 (green), anti-MCT4 (red), and DAPI (blue). Scale bar, 100  $\mu$ m. (C and D) Electron microscopy of the labyrinthine layer of the placenta. Sections of the placenta in E13.5 *Atp11a<sup>+/+</sup>* and *Atp11a<sup>klk</sup>* mice were analyzed by transmission electron microscopy (C) or scanning electron microscopy (D). The boxed area (Upper) was enlarged in the Bottom in (C). The arrowheads indicate degenerated nuclei. The cell boundary was surrounded by an orange line in D. Scale bar, 100  $\mu$ m (C, Upper), 20  $\mu$ m (C, Lower), 10  $\mu$ m (D). End, endothelial cell; mono-TP, mononuclear trophoblasts. (E) Cryosections from the E13.5 *Atp11a<sup>+/+</sup>* and *Atp11a<sup>klk</sup>* placenta were stained with TUNEL. Red, TUNEL; blue, DAPI. Scale bar, 250  $\mu$ m. Right: Total TUNEL-positive area was quantified with three sections per placenta, and the ratio against the DAPI-positive area in the labyrinthine layer was plotted ( $n = 3$  for *Atp11a<sup>+/+</sup>* or *Atp11a<sup>klk</sup>* and  $n = 6$  for *Atp11a<sup>klk</sup>*).  $P$  values calculated by Student's  $t$  test are shown. (F) RNA from the E13.5 *Atp11a<sup>+/+</sup>* (+/+) and *Atp11a<sup>klk</sup>* (klk) placenta ( $n = 3$  for each) was subjected to real-time RT-PCR to assess the mRNA levels of the indicated genes. The average values were plotted with SD (bars).

its solvent dimethyl sulfoxide (DMSO) (0.05%). Staining with anti-E-cadherin antibody (Ab) indicated that a high level of E-cadherin was present at the site of cell-to-cell contact in aggregated BeWo cells in control DMSO-treated cells (Fig. 5D). As reported by Coutifaris et al. (34), the treatment of wild-type BeWo cells with forskolin strongly reduced the intensity of E-cadherin or even removed it at several locations, suggesting that these cells underwent cell fusion. On the other hand, the expression of E-cadherin in *DKO*-BeWo cells remained after the forskolin treatment, while it disappeared in forskolin-treated *DKO*-BeWo-ATP11A cells. Observations by scanning electron microscopy indicated that the area size of wild-type BeWo cells increased 4.1-fold from 565 to 2,299  $\mu$ m<sup>2</sup> after the treatment

with forskolin for 48 h, while the perimeter length increased 2.2-fold from 105 to 228  $\mu$ m (Fig. 5E). Similar increases in the area size and perimeter length were observed in forskolin-treated *DKO*-ATP11A cells but not *DKO*-BeWo cells. Omata et al. (35) previously reported that the forskolin-induced fusion of BeWo cells was accompanied by the expression of a number of genes related to cell differentiation or cell fusion. Real-time RT-PCR indicated that the expression of the *SYNCYTIN2* gene that can be up-regulated by forskolin treatment before cell fusion increased to a similar extent between wild-type and *DKO*-BeWo cells after the forskolin treatment (Fig. 5F). The up-regulation of the *DYSFERIN* gene that occurs after cell fusion (35) was less pronounced in *DKO*-BeWo cells, supporting a role of the plasma

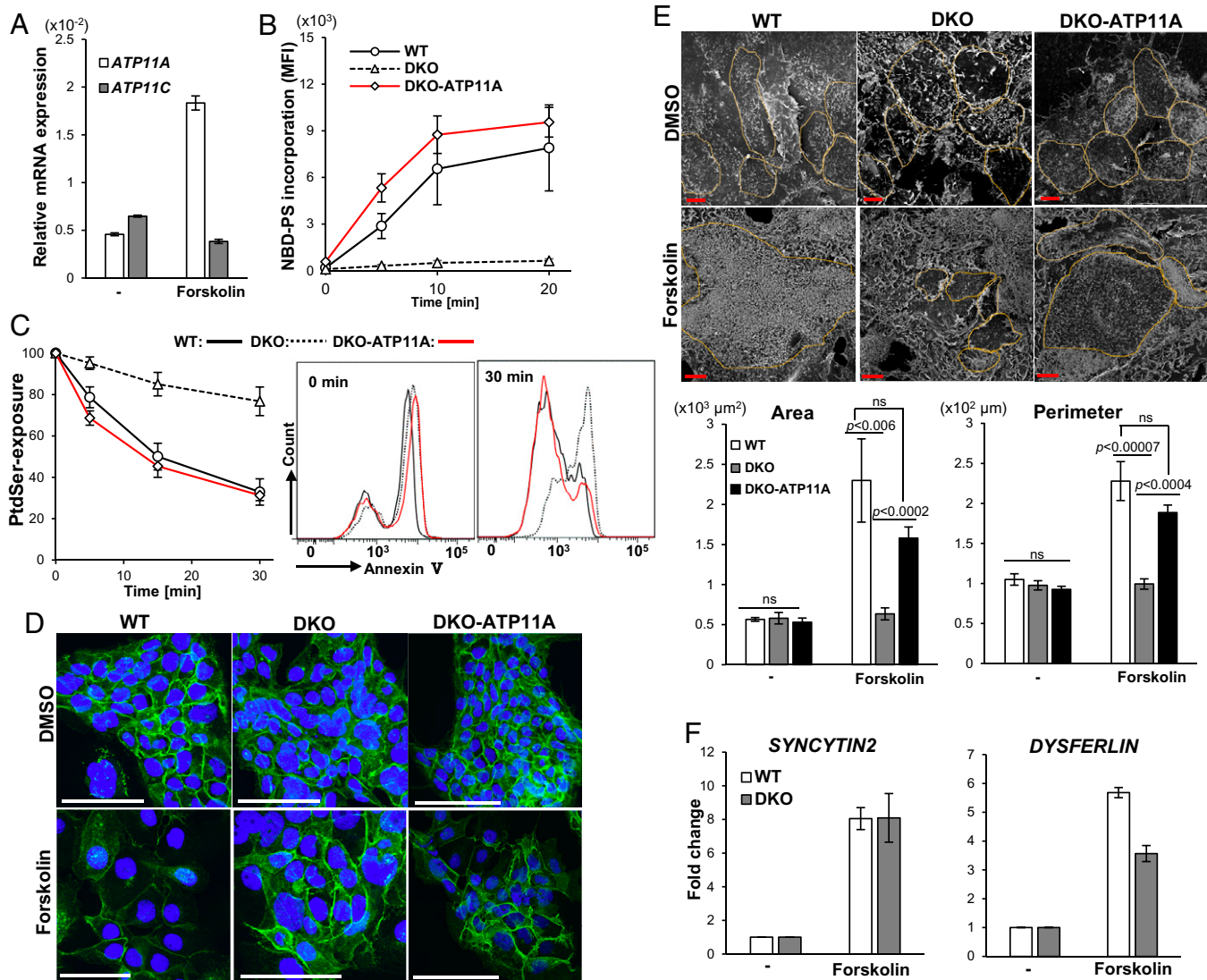


**Fig. 5.** Inefficient cell fusion of human BeWo cells lacking ATP11A and ATP11C. (A) Human BeWo cells were treated for 48 h with 20  $\mu$ M forskolin. In forskolin-treated or untreated cells, mRNAs for *ATP11A* and *ATP11C* were quantified by real-time RT-PCR, and their levels are shown relative to that of  $\beta$ -*ACTIN* (*ACTB*). The experiment was performed three times, and average values are shown with SD (bars). (B) Wild-type (WT) BeWo, *DKO*-BeWo, and *DKO-ATP11A* cells were incubated at 15  $^{\circ}$ C with NBD-PS for the indicated period, treated with fatty acid-free BSA, and subjected to flow cytometry. Experiments were performed three times, and the average value of mean fluorescence intensity of incorporated NBD-PS in the Sytox blue-negative population was plotted with SD (bar). (C) Reestablishment of the asymmetrical distribution of PtdSer. WT-BeWo, *DKO*, and *DKO-ATP11A* cells were treated at 15  $^{\circ}$ C for 5 min with 5  $\mu$ M ionomycin and incubated at 25  $^{\circ}$ C for the indicated time in the culture medium containing EGTA and BAPTA-AM. The exposure of PtdSer was then analyzed by the binding of Cy5-annexin V. Experiments were performed three times, and the average percentage of the annexin V-positive population in PI-negative cells was plotted with SD. (D–F) Forskolin-induced cell fusion. WT-BeWo, *DKO*, and *DKO-ATP11A* cells were treated at 37  $^{\circ}$ C for 48 h with 20  $\mu$ M forskolin. (D) Cells were stained with anti-E-cadherin Ab (green) and DAPI (blue). Scale bar, 100  $\mu$ m. (E) Cells were observed by scanning electron microscopy. Scale bar, 10  $\mu$ m. The size of the cellular area and perimeter length were assessed for at least six randomly selected cells. Lower: Mean value  $\pm$  SEM (bar). Statistical analyses were performed using Student's *t* test, and *P* values are shown. ns stands for “not significant”. ns, not significant. (F) mRNA levels for *SYNCYTIN 2* and *DYSFERLIN* were assessed by real-time RT-PCR and normalized to *ACTB* mRNA. Experiments were performed three times, and the average values were presented with SD (bars).

membrane flippase, ATP11A or ATP11C, in the fusion of BeWo cells.

## Discussion

The mouse P4-ATPase family comprises 14 members, with ATP11A, ATP11B, and ATP11C belonging to class 6 of the family (6). We herein demonstrated that a global deficiency of *Atp11a* caused embryonic lethality and mutant mice died after E14.5, possibly due to heart failure. As previously reported in embryonic lethal mutant mice with heart failure (21–23, 36), the placenta was abnormal or poorly developed in *Atp11a*-null mice. Organogenesis of the mouse heart, accompanied by the

proliferation of cardiac myocytes to thicken the ventricular wall, occurs between E8.5 and E14.5 (37, 38). Since the proliferation of cardiac myocytes is strongly affected by blood flow and hemodynamics (39), a decrease in blood flow due to placental defects may cause abnormal heart development in the embryo.

In contrast to the global *Atp11a* deficiency, the epiblast-specific *Atp11a*-null mutation had no apparent effect on mouse development. The mice live healthy at least at the age of 16 mo. ATP11A, ATP11B, and ATP11C have 58 to 64% identities on the amino acid sequence and translocate PtdSer when they are reconstituted in liposomes (40). ATP11A and ATP11B, but not ATP11C, are highly expressed in placental trophoblasts

(Expression Atlas: <https://www.ebi.ac.uk/gxa/home>). In contrast, ATP11A and ATP11C are ubiquitously expressed in other tissues (8). ATP11A and ATP11C are present at the plasma membrane, while ATP11B is localized intracellularly or in early or recycling endosomes (8, 41). The severe phenotype of the *Atp11a*-null placenta indicated that ATP11B, a flippase at endosomes, was unable to compensate for the null mutation of the plasma membrane flippase (ATP11A), whereas ATP11C at the plasma membranes in the embryonal cells can compensate for the *Atp11a*-null mutation for the development of embryos.

In various biological processes, live cells transiently expose PtdSer to the cell surface (4). Differentiating human trophoblasts expose PtdSer on the cell surface (42), and the Ab against PtdSer inhibits the forskolin-induced fusion of BeWo cells (43). In addition, a high titer of anti-PtdSer Ab in the serum is often associated with recurrent early or late abortions due to the inefficient development of the placenta (44). Based on these findings, Chernomordik's group proposed that PtdSer functions as a "fuse me" signal (45, 46). Accordingly, Zhang et al. (47) recently claimed that TMEM16F, a  $\text{Ca}^{2+}$ -dependent phospholipid scramblase (33), was responsible for the exposure of PtdSer during the fusion of trophoblasts. However, the normal development of *Tmem16f*-null embryos (48) may reject its involvement in this process.

The development of syncytiotrophoblasts was inefficient in the *Atp11a*-null placenta, which is similar to the phenotype reported in mice deficient in *Syncytin-A* (28), supporting the role of ATP11A in the efficient fusion of trophoblasts. The function of plasma membrane flippases (ATP11A and ATP11C) is to swiftly internalize PtdSer exposed on the cell surface (16). PtdSer irreversibly exposed on the cell surface due to the lack of flippases functions as an eat-me signal not only for apoptotic cells but also for live cells (16). We previously demonstrated that B-cell lymphopenia in *Atp11c*-deficient mice was due to the engulfment by macrophages of precursor B cells that failed to internalize the exposed PtdSer due to the lack of plasma membrane flippases (16). On the other hand, the lack of the PtdSer-dependent engulfment system (MerTK and Axl tyrosine kinases) did not rescue the embryonic lethality of *Atp11a*-null mice (*SI Appendix*, Table S1). It is likely that the prolonged exposure of PtdSer prevented cell fusion or that PtdSer exposed on the cell surface had to return to the inner leaflet of the plasma membrane to complete cell fusion. PtdSer has been shown to change the surface charge of membranes and regulates protein localization (49). In trophoblasts undergoing fusion, intracellular annexin V localizes via PtdSer between mononuclear trophoblasts and syncytiotrophoblasts to form an adherent junction composed of E-cadherin,  $\beta$ -catenin, and  $\alpha$ -catenin (50). A low concentration of PtdSer at the inner leaflet of plasma membranes due to the lack of the flippase (ATP11A) may have resulted in an inefficient adherent junction. A large number of dying trophoblasts in the labyrinthine layer of the *Atp11a*-null placenta suggests that unfused differentiated trophoblasts cannot survive, which is consistent with previous findings on anti-phospholipid-antibody-treated trophoblasts (51).

The involvement of PtdSer in cell fusion has been suggested not only for trophoblasts but also for myoblasts, osteoclasts, and egg/sperm fusion (45). Two groups recently established mouse myoblasts that lack CDC50A, a shared subunit of multiple P4-ATPases, or ATP11A, and reported contradictory findings (52, 53). One group showed that multiple P4-ATPases were required for the efficient fusion of C2C12 cells (53), while the other claimed that a deficiency in *Cdc50a* or *Atp11a* caused

the uncontrolled fusion of myoblasts in vitro and in vivo (52). The present results on trophoblasts are consistent with the former findings; however, we cannot rule out the possibility that myoblasts and trophoblasts use different mechanisms for fusion. The exposure of PtdSer has been proposed to serve as a fuse-me signal in the fusion process of various cells (45). The present study showed that the distribution of PtdSer needs to be tightly regulated for efficient fusion, at least for the formation of syncytiotrophoblasts. In order for PtdSer to serve as an eat-me signal, it binds to a specific receptor or receptors on macrophages and activates their engulfment system (54). Further studies are needed to identify which scramblase family members (TMEM16, XKR, or others) are responsible for exposing PtdSer in the fusion process and also to elucidate the molecular mechanisms by which PtdSer is recognized in order to activate the fusion process.

## Materials and Methods

**Mice.** C57BL/6N mice and MRL-*lpr/lpr* mice were obtained from Japan SLC. *Atp11a*<sup>+/*komp*</sup> mice (*Atp11a*<sup>tm1a(KOMP)/Wtsi</sup>) were from the Mutant Mouse Resource and Research Centers. *SI Appendix*, Fig. S1 shows the structure of the *Atp11a*<sup>+/*komp*</sup> allele. *Atp11a*<sup>lox/+</sup> mice in which two *loxP* elements flanked exons 7 and 8 of the *Atp11a* gene were prepared by crossing *Atp11a*<sup>+/*komp*</sup> mice with mice carrying the CAG-FLPe gene [C57BL/6-Tg(CAG-flpe)36lto/ItorBrc] (Riken).  *$\alpha$ Mhc-Cre* mice [B6.FVB-Tg(Myh6-cre)2182Mds/J] carrying the *Cre* gene under the promoter of  *$\alpha$ Mhc* were from the Jackson Laboratory. *Sox2-Cre* mice (B6N.Cg-*Edil3*<sup>Tg(Sox2-cre)1AmdJ</sup>) in which *Cre* is under the control of the *SRY-box containing gene 2* promoter were from the Jackson Laboratory through R. Nishinakamura (Kumamoto University). All mice were housed in a specific pathogen-free facility at the Research Institute for Microbial Diseases, Osaka University. The Ethics Review Committee at Osaka University approved all mouse studies.

Mouse pregnancy was checked by vaginal plugs and confirmed by weight gain (55). The morning when a vaginal plug was observed was noted as E0.5. In some cases, embryos were generated by in vitro fertilization as previously described (56). Genotyping was performed with DNA prepared from tail snips according to the protocol in the Jackson Laboratory (<https://www.jax.org/jax-mice-and-services/customer-support/technical-support/genotyping-resources/dna-isolation-protocols>) using the primers described in *SI Appendix*, Table S2.

**Cell Lines, Plasmids, Ab, and Reagents.** Human HEK293T (American Type Culture Collection CRL-3216) and BeWo (Riken RCB3678) cells were maintained in Dulbecco's modified eagle medium (DMEM) containing 10% fetal calf serum (FCS) (Gibco) and in Ham's F-12 medium containing 15% FCS, respectively. Mouse cardiac myocytes were prepared as previously described (57). In brief, the hearts of E13.5 embryos were washed with phosphate-buffered saline (PBS), placed in 300  $\mu$ L of enzyme solution [350  $\mu$ g/mL pancreatin (Nacalai Tesque) in 136.9 mM NaCl, 11.1 mM D-glucose, 2.6 mM KCl, 41.7 mM  $\text{NaH}_2\text{PO}_4$ , and 11.9 mM  $\text{NaHCO}_3$ ], and incubated at 37 °C for 10 min. The solution excluding the undigested heart was transferred to a new tube, mixed with 300  $\mu$ L of DMEM containing 10% FCS, and spun at 1,000 rpm for 10 min. Precipitated myocytes were suspended in DMEM-10% FCS. Fresh enzyme solution was concurrently added to the heart and incubated at 37 °C for 10 min. This procedure (the treatment with enzyme solution and collection by centrifugation) was repeated five to eight times, and all myocytes were combined.

The plasmids pMAL-p2x and pGEX-5x-1 were purchased from New England Biolabs and GE Healthcare, respectively. pX459v2 was from Addgene. pCMV-VSV-G and pCAG-HIVgp were from Riken. The pLVISIN-EF-1 $\alpha$ -Pur vector was from Takara Bio.

A horseradish peroxidase (HRP)-labeled mouse anti-FLAG mAb (clone M2) and chicken anti-rat Mct1 Ab were purchased from Sigma-Aldrich. HRP-goat anti-mouse immunoglobulin (Ig)G<sub>2a</sub> heavy-chain Ab, rabbit anti-human cTnT mAb (clone EPR3696), Alexa Fluor 568-donkey anti-rat IgG (Heavy and Light chains, H+L) preadsorbed Ab, and Alexa Fluor 568-donkey anti-mouse IgG (H+L) Ab were from Abcam. Rat anti-mouse E-cadherin mAb (clone ECCD-2), Alexa Fluor 488-goat anti-rat IgG (H+L) Ab, Alexa Fluor 488-goat anti-chicken

IgY (H+L) Ab, and Alexa Fluor 568-goat anti-rabbit IgG (H+L) Ab were from Invitrogen. HRP-goat anti-mouse IgG Ab was purchased from Dako Agilent. Mouse anti-human Mct4 mAb (clone D-1) was from Santa Cruz.

NBD-PS was purchased from Avanti Polar Lipids. X-gal was from Fujifilm Wako Pure Chemical Co. SPiDER- $\beta$ Gal, DAPI, and O,O'-Bis(2-aminophenyl)ethylene-neglycol-*N,N,N',N'*-tetraacetic acid, tetraacetoxymethyl ester (BAPTA-AM) were from Dojindo Molecular Technologies. Forskolin and ionomycin were from Sigma-Aldrich and Merck, respectively. Cy5-labeled annexin V was purchased from BioVision. Accutase was from Nacalai Tesque.

**mAb against Mouse ATP11A.** A hybridoma (clone 4-C11) producing mAb against mouse ATP11A was established by immunizing MRL-*lpr/lpr* mice as previously described (58) with a recombinant mouse ATP11A protein. In brief, two regions of mouse ATP11A (amino acids 427 to 513 and 408 to 892) were fused to glutathione *S*-transferase (GST) and maltose-binding protein (MBP), respectively, produced in *Escherichia coli* BL21 and were purified using glutathione Sepharose (GE Healthcare) and amylose resin (New England Biolabs), respectively.

Female MRL-*lpr/lpr* mice at the age of 4 wk were injected subcutaneously twice at a 2-wk interval with 50  $\mu$ g of GST-ATP11A mixed with TiterMax Gold (TiterMax). Mice were further immunized by intraperitoneal injections of 50  $\mu$ g of the protein in PBS at a 3-d interval. After six injections, the Ab serum titer plateaued. Lymphocytes were prepared from the popliteal and inguinal lymph nodes 1 d after the last injection and fused with NSO<sup>Bcl-2</sup> myeloma (59). Hybridomas were cultured at 37 °C in DMEM containing 10% FCS, 10% NCTC-109 (Gibco), 1% nonessential amino acids, 5.5 U/mL human IL-6, 100  $\mu$ M hypoxanthine, 0.4  $\mu$ M aminopterin, and 16  $\mu$ M thymidine, and screened by enzyme-linked immunosorbent assay (ELISA) using MBP-fused ATP11A. A positive hybridoma (clone 4-C11) was cultured in ASF medium 104N (Ajinomoto), and the Ab was purified by (NH<sub>4</sub>)<sub>2</sub>SO<sub>4</sub> precipitation, followed by dialysis against PBS. The Ig subclass of the 4-C11 mAb, identified by the IsoStrip Mouse Monoclonal Antibody Isotyping kit (Roche Diagnostics), was IgG<sub>2a</sub>. In ELISA to assess the Ab titer, 96-well plates were coated with 50 ng of MBP-ATP11A. Samples were serially diluted with PBS containing 1% bovine serum albumin (BSA) and 0.05% Tween 20, added to the wells, and incubated at 4 °C for 12 to 16 h. The assay was developed with HRP-goat anti-mouse IgG, and peroxidase activity was detected with a peroxidase-detecting kit (Sumiron, Sumitomo) using *o*-phenylenediamine as a substrate. Absorbance at 492 nm was measured using a microplate reader (Infinite M200, Tecan).

**Real-Time RT-PCR and Western Blotting.** RNA was isolated from tissues and cells as previously described (60) and reverse transcribed using a High Capacity RNA-to-cDNA kit (Applied Biosystems). Real-time PCR was performed using the LightCycler system (Roche Diagnostics) with the primers described in *SI Appendix, Table S2*. Regarding Western blotting, mouse tissues were suspended in radio-immunoprecipitation assay (RIPA) buffer [50 mM Hepes-NaOH (pH 7.6), 150 mM NaCl, 1 mM ethylene glycol tetraacetic acid (EGTA), 1.5 mM MgCl<sub>2</sub>, 10% glycerol, 1% Triton X-100, 0.1% sodium dodecyl sulfate (SDS), and 0.5% sodium deoxycholate] containing 1% protease inhibitor mixture (Nacalai Tesque), broken by sonication at 4 °C, and centrifuged at 20,000  $\times$  *g* for 30 min. The supernatants (1.0 to 8.5  $\mu$ g of protein) were separated by 7.5% SDS-polyacrylamide gel electrophoresis (PAGE) (Extra PAGE One Precast Gel, Nacalai Tesque) and transferred to polyvinylidene difluoride (PVDF) membranes (Merck). After incubating at room temperature for 1 h in buffer A (PBS containing 0.05% Tween 20 and 1 to 5% skim milk), the membrane was incubated at 4 °C for 12 to 16 h with 0.2  $\mu$ g/mL 4-C11 mAb in buffer A, followed by incubation for 1 h with 1  $\mu$ g/mL HRP-goat anti-mouse IgG<sub>2a</sub> heavy-chain Ab. HRP activity was visualized using Western LightningPlus-ECL (PerkinElmer) and detected by LAS4000 (GE Healthcare).

**Histological Analyses and TUNEL Staining.** In the histological analysis, tissues were fixed at room temperature for 48 h in PBS-4% paraformaldehyde (PFA), soaked overnight in 70% ethanol, dehydrated, embedded in paraffin, sliced into 4- to 6- $\mu$ m-thick sections, and mounted on glass slides. Samples were then stained with hematoxylin and eosin (H&E) and observed under a fluorescence microscope. Regarding immunohistological staining, placentas were mounted in optimal cutting temperature (OCT) compound (Sakura Finetek), frozen at -80 °C, and sectioned at a thickness of 5  $\mu$ m. After fixing with 4.0% PFA

for 20 min, cells were permeabilized by treatment with 0.1% Triton X-100 at room temperature for 5 min. Sections were incubated for 60 min with 2  $\mu$ g/mL chicken anti-rat Mct1 Ab and 5  $\mu$ g/mL mouse anti-human Mct4 mAb, followed by incubation with Alexa Fluor 488-goat anti-chicken IgY Ab and Alexa Fluor 568-donkey anti-mouse IgG (H+L) Ab. Samples were mounted on FluorSave and observed by confocal fluorescence microscopy (IX81, Olympus).

In TUNEL staining, placentas were fixed at room temperature for 48 h in PBS-4% PFA, dehydrated, embedded in paraffin, and sliced into 6- $\mu$ m-thick sections. TUNEL staining was performed using the In Situ Cell Death Detection kit, tetramethylrhodamine (TMR) red (Roche Diagnostics). Sections were counterstained with 1  $\mu$ g/mL DAPI, mounted on FluorSave, and observed by fluorescence microscopy (BioRevo BZ-9000, Keyence). TUNEL-positive areas were quantitated using ImageJ software (<https://imagej.nih.gov/ij/>).

**X-Gal and SPiDER- $\beta$ Gal Staining.** Tissues were fixed at 4 °C for 1 h in PBS containing 4% PFA and washed with X-gal buffer (PBS containing 2 mM MgCl<sub>2</sub>, 0.02% Nonidet P-40, and 0.01% sodium deoxycholate). After pricking several places with a needle, tissues were immersed in 2 mg/mL X-gal in X-gal buffer containing 5 mM potassium ferricyanide and incubated in the dark at 37 °C for 24 to 48 h. Tissues were fixed at room temperature for 48 h in 4% PFA, soaked overnight in 70% ethanol, and dehydrated. Samples were then embedded in paraffin using CT-Pro20 (Japan Genetics) and sliced into 12- $\mu$ m-thick sections using a microtome (RM2245, Leica). After being deparaffinized and rehydrated, samples were counterstained with 0.1% nuclear fast red (Sigma) in 5% (wt/vol) aluminum sulfate and observed on a fluorescence microscope.

In SPiDER- $\beta$ Gal staining (19), mouse cardiomyocytes cultured on fibronectin-coated glass coverslips were fixed at room temperature for 10 min in PBS-0.2% PFA and incubated at 37 °C for 1 to 2 h in PBS containing 3 to 5  $\mu$ M SPiDER- $\beta$ Gal and 0.1% Triton X-100. Samples were further incubated at room temperature for 60 min in PBS-2% BSA and stained with 2  $\mu$ g/mL rabbit anti-human cTnT Ab, followed by incubation with 1  $\mu$ g/mL Alexa Fluor 568-goat anti-rabbit IgG Ab. Samples were stained with 1  $\mu$ g/mL DAPI, mounted with FluorSave, and observed under a confocal fluorescence microscope (IX83, Olympus).

**Electron Microscopy.** On day 13 postmating, pregnant mice were anesthetized by an intraperitoneal injection of three anesthetics [medetomidine hydrochloride (Zenoaq), midazolam (Astellas Pharma), and butorphanol (Meiji Seika Pharma)] and subjected to cardiac perfusion with 200 to 300 mL of 0.1 M sodium phosphate buffer (pH 7.4) containing 2% glutaraldehyde and 2% PFA. The placenta was removed, fixed at 4 °C overnight, and left at room temperature for 3 d in 0.1 M sodium phosphate buffer (pH 7.4). Samples were postfixed with 1% OsO<sub>4</sub> at 4 °C for 2 h and dehydrated. Samples were incubated twice in propylene oxide (PO) for 20 min, in a 3:1 mixture of PO and epoxide for 1 h, in a 1:3 mixture of PO and epoxide for 1 h, and in epoxide overnight. After incubating in epoxide at 60 °C for 3 d, ultrathin sections (thickness of 70 to 80 nm) were prepared with an Ultracut UCT ultramicrotome (Leica), stained with uranyl acetate and lead citrate, and observed with a transmission electron microscope (H-7650, Hitachi High-Technologies) or scanning electron microscope (Helios NanoLab 660, Field Electron and Ion Company).

**Gene Editing and Transformation of Cell Lines.** The *ATP11A* and *ATP11C* genes in BeWo cells were knocked out using the CRISPR-Cas9 system (9, 32). Complementary oligonucleotides carrying the single-guide (sg)RNA target sequence for human *ATP11A* and *ATP11C* genes (*SI Appendix, Table S2*) were annealed and ligated into pX459v2. Plasmid DNA was introduced into BeWo cells using FuGENE<sup>®</sup> HD (Promega). Single clones were isolated by limiting dilutions and genotyped by sequencing the target region of chromosomal DNA. Human *ATP11A* cDNA (NM\_032189.4) was previously described (8). The DNA fragment for Flag-tagged *ATP11A* was inserted into pLVISIN-EF-1 $\alpha$  Neo and introduced into HEK293T cells with pCAG-HIVgp and pCMV-VSV-G-RSV-rev using Fugene6 (Promega). After culturing for 2 d, the virus in the supernatant was collected with the Lenti-X Concentrator (Takara Bio) and used to infect *DKO*-BeWo cells. Transformants were selected with 250  $\mu$ g/mL G418.

**Flippase Assay.** Flippase activity for endogenous PtdSer or exogenous PtdSer analog was assessed as previously described (16). In brief, 5.0  $\times$  10<sup>4</sup> BeWo cells in a 12-well plate were cultured overnight, washed with Hanks' balanced salt solution (HBSS) (-) without phenol red (buffer B), and incubated at 15 °C with

1  $\mu\text{M}$  NBD-PS in 200  $\mu\text{L}$  of buffer B. Cells were incubated at 4 °C for 1 min in buffer B containing 5 mg/mL fatty acid-free BSA, treated at room temperature for 3.5 min with Accutase, mixed with 200  $\mu\text{L}$  of buffer B containing 5 mg/mL fatty acid-free BSA and 500 nM Sytox blue (Thermo Fisher Scientific), and analyzed by fluorescence-activated cell sorting (FACS) Canto II (BD Biosciences). Data were assessed by FlowJo software (BD Biosciences). To evaluate flippase activity for endogenous PtdSer, BeWo cells were cultured as above, detached by a treatment with Accutase, and collected by centrifugation at 200  $\times g$  at 4 °C for 2 min. Cells were then treated at 15 °C for 5 min with 5  $\mu\text{M}$  ionomycin in 800  $\mu\text{L}$  of annexin V buffer [10 mM Hepes-NaOH (pH 7.6), 140 mM NaCl, 2.5 mM  $\text{CaCl}_2$ ] to expose PtdSer. Cells were collected by centrifugation, resuspended in 600  $\mu\text{L}$  of DMEM containing 15% FCS, 5 mM EGTA, and 20  $\mu\text{M}$  BAPTA-AM, and incubated at 25 °C. Cells were then suspended in 400  $\mu\text{L}$  of annexin V buffer containing 1,000-fold diluted Cy5-labeled annexin V and 5  $\mu\text{g/mL}$  propidium iodide (PI; Merck) and analyzed by FACS Canto II.

**Cell Fusion with BeWo Cells.** The fusion of BeWo cells was performed according to Omata et al. (35). In brief,  $1 \times 10^5$  BeWo cells in a six-well plate were treated for 48 h with 20  $\mu\text{M}$  forskolin with a medium change at 24 h. Cell fusion was evaluated by immunohistochemical staining followed by morphological observations and by scanning electron microscopy. Cells were fixed with 4% PFA, permeabilized with 0.1% Triton X-100, and stained at room temperature for 1 h with 2  $\mu\text{g/mL}$  rat anti-mouse E-cadherin mAb, followed by incubation with 1  $\mu\text{g/mL}$  Alexa Fluor 488-goat anti-rat IgG (H+L) Ab. Samples were counterstained with 5  $\mu\text{g/mL}$  DAPI, mounted by FluorSave, and observed under a confocal fluorescence microscope.

Regarding scanning electron microscopy, cells were fixed with 2.5% glutaraldehyde in 0.1 M phosphate buffer (pH 7.4), postfixed with 2%  $\text{OsO}_4$ , and dehydrated with a graded series of ethanol. After treatment with *t*-butyl alcohol, samples were freeze-dried with a freeze dryer (VFD-30, Vacuum Device) and mounted on aluminum stubs with carbon paste. Dried specimens were coated with osmium with a Neoc-Pro osmium coater (Meiwaofosis) and observed under the field-emission scanning electron microscope (JSM-IT800, JEOL). To estimate cellular areas and perimeters, cell boundaries were traced and analyzed using ImageJ software. Data were expressed as the area (in squared micrometers) and perimeter (in micrometers) of the syncytium surrounded by the cell boundary.

**Statistical Analysis.** Data obtained from each experiment were expressed as the mean  $\pm$  SEM or the mean  $\pm$  SD. Statistical analyses were performed using Student's *t* test.

**Data Availability.** All study data are included in the article and/or *SI Appendix*.

**ACKNOWLEDGMENTS.** We thank M. Kamada for secretarial assistance. This work was supported in part by grants-in-aid from the Japan Society for the Promotion of Science (21H04770) to S.N.

Author affiliations: <sup>a</sup>Laboratory of Biochemistry and Immunology, Immunology Frontier Research Center, Osaka University, Suita 565-0871, Japan; <sup>b</sup>Department of Cellular and Molecular Pharmacology, Graduate School of Medicine, Juntendo University, Tokyo 113-8421, Japan; <sup>c</sup>Department of Cellular and Neuropathology, Graduate School of Medicine, Juntendo University, Tokyo 113-8421, Japan; and <sup>d</sup>Center for Infectious Disease Education and Research, Osaka University, Suita 565-0871, Japan

1. T. Harayama, H. Riezman, Understanding the diversity of membrane lipid composition. *Nat. Rev. Mol. Cell Biol.* **19**, 281–296 (2018).
2. P. A. Leventis, S. Grinstein, The distribution and function of phosphatidylserine in cellular membranes. *Annu. Rev. Biophys.* **39**, 407–427 (2010).
3. R. B. Birge et al., Phosphatidylserine is a global immunosuppressive signal in efferocytosis, infectious disease, and cancer. *Cell Death Differ.* **23**, 962–978 (2016).
4. E. M. Bevers, P. L. Williamson, Getting to the outer leaflet: Physiology of phosphatidylserine exposure at the plasma membrane. *Physiol. Rev.* **96**, 605–645 (2016).
5. S. Nagata, J. Suzuki, K. Segawa, T. Fujii, Exposure of phosphatidylserine on the cell surface. *Cell Death Differ.* **23**, 952–961 (2016).
6. J. P. Andersen et al., P4-ATPases as phospholipid flippases—Structure, function, and enigmas. *Front. Physiol.* **7**, 275 (2016).
7. R. L. López-Marqués, L. Theorin, M. G. Palmgren, T. G. Pomorski, P4-ATPases: Lipid flippases in cell membranes. *Pflügers Arch.* **466**, 1227–1240 (2013).
8. K. Segawa, S. Kurata, S. Nagata, Human type IV P-type ATPases that work as plasma membrane phospholipid flippases and their regulation by caspase and calcium. *J. Biol. Chem.* **291**, 762–772 (2016).
9. K. Segawa et al., Caspase-mediated cleavage of phospholipid flippase for apoptotic phosphatidylserine exposure. *Science* **344**, 1164–1168 (2014).
10. H. Nakanishi et al., Crystal structure of a human plasma membrane phospholipid flippase. *J. Biol. Chem.* **295**, 10180–10194 (2020).
11. O. M. Siggs et al., The P4-type ATPase ATP11C is essential for B lymphopoiesis in adult bone marrow. *Nat. Immunol.* **12**, 434–440 (2011).
12. O. M. Siggs, B. Schnabl, B. Webb, B. Beutler, X-linked cholestasis in mouse due to mutations of the P4-ATPase ATP11C. *Proc. Natl. Acad. Sci. U.S.A.* **108**, 7890–7895 (2011).
13. M. Yabas et al., Mice deficient in the putative phospholipid flippase ATP11C exhibit altered erythrocyte shape, anemia, and reduced erythrocyte life span. *J. Biol. Chem.* **289**, 19531–19537 (2014).
14. M. Yabas et al., ATP11C is critical for the internalization of phosphatidylserine and differentiation of B lymphocytes. *Nat. Immunol.* **12**, 441–449 (2011).
15. N. Arashiki et al., ATP11C is a major flippase in human erythrocytes and its defect causes congenital hemolytic anemia. *Haematologica* **101**, 559–565 (2016).
16. K. Segawa et al., Phospholipid flippases enable precursor B cells to flee engulfment by macrophages. *Proc. Natl. Acad. Sci. U.S.A.* **115**, 12212–12217 (2018).
17. K. Takata, K. Fujikura, B.-C. Shin, Ultrastructure of the rodent placental labyrinth: A site of barrier and transport. *J. Reprod. Dev.* **43**, 13–24 (1997).
18. D. Hu, J. C. Cross, Development and function of trophoblast giant cells in the rodent placenta. *Int. J. Dev. Biol.* **54**, 341–354 (2010).
19. T. Doura et al., Detection of LacZ-positive cells in living tissue with single-cell resolution. *Angew. Chem. Int. Ed. Engl.* **55**, 9620–9624 (2016).
20. R. Agah et al., Gene recombination in postmitotic cells. Targeted expression of Cre recombinase provokes cardiac-restricted, site-specific rearrangement in adult ventricular muscle in vivo. *J. Clin. Invest.* **100**, 169–179 (1997).
21. V. Perez-Garcia et al., Placentation defects are highly prevalent in embryonic lethal mouse mutants. *Nature* **555**, 463–468 (2018).
22. W. J. Weninger et al., Phenotyping structural abnormalities in mouse embryos using high-resolution episcopic microscopy. *Dis. Model. Mech.* **7**, 1143–1152 (2014).
23. N. A. Karp, R. Heller, S. Yaacoby, J. K. White, Y. Benjamini, Improving the identification of phenotypic abnormalities and sexual dimorphism in mice when studying rare event categorical characteristics. *Genetics* **205**, 491–501 (2017).
24. H. B. Wood, V. Episkopou, Comparative expression of the mouse Sox1, Sox2 and Sox3 genes from pre-gastrulation to early somite stages. *Mech. Dev.* **86**, 197–201 (1999).
25. M. V. Zappone et al., Sox2 regulatory sequences direct expression of a (beta)-geo transgene to telencephalic neural stem cells and precursors of the mouse embryo, revealing regionalization of gene expression in CNS stem cells. *Development* **127**, 2367–2382 (2000).
26. S. Hayashi, P. Lewis, L. Pevny, A. P. McMahon, Efficient gene modulation in mouse epiblast using a Sox2Cre transgenic mouse strain. *Mech. Dev.* **119** (suppl. 1), S97–S101 (2002).
27. A. Nagai, K. Takebe, J. Nio-Kobayashi, H. Takahashi-Iwanaga, T. Iwanaga, Cellular expression of the monocarboxylate transporter (MCT) family in the placenta of mice. *Placenta* **31**, 126–133 (2010).
28. A. Dupressoir et al., Syncytin-A knockout mice demonstrate the critical role in placentation of a fusogenic, endogenous retrovirus-derived, envelope gene. *Proc. Natl. Acad. Sci. U.S.A.* **106**, 12127–12132 (2009).
29. M. Ueno et al., c-Met-dependent multipotent labyrinth trophoblast progenitors establish placental exchange interface. *Dev. Cell* **27**, 373–386 (2013).
30. B. Marsh, R. Bleiloch, Single nuclei RNA-seq of mouse placental labyrinth development. *eLife* **9**, e60266 (2020).
31. B. Wice, D. Menton, H. Geuze, A. L. Schwartz, Modulators of cyclic AMP metabolism induce syncytiotrophoblast formation in vitro. *Exp. Cell Res.* **186**, 306–316 (1990).
32. F. A. Ran et al., Genome engineering using the CRISPR-Cas9 system. *Nat. Protoc.* **8**, 2281–2308 (2013).
33. J. Suzuki, M. Umeda, P. J. Sims, S. Nagata, Calcium-dependent phospholipid scrambling by TMEM16F. *Nature* **468**, 834–838 (2010).
34. C. Coutifaris et al., E-cadherin expression during the differentiation of human trophoblasts. *Development* **113**, 767–777 (1991).
35. W. Omata, W. E. Ackerman IV, D. D. Vandre, J. M. Robinson, Trophoblast cell fusion and differentiation are mediated by both the protein kinase C and a pathways. *PLoS One* **8**, e81003 (2013).
36. E. O. Maruyama et al., Extraembryonic but not embryonic SUMO-specific protease 2 is required for heart development. *Sci. Rep.* **6**, 20999 (2016).
37. S. Gessert, M. Kühl, The multiple phases and faces of wnt signaling during cardiac differentiation and development. *Circ. Res.* **107**, 186–199 (2010).
38. M. J. Foglia, K. D. Poss, Building and re-building the heart by cardiomyocyte proliferation. *Development* **143**, 729–740 (2016).
39. K. L. Thornburg, P. F. O'Tierney, S. Louey, Review: The placenta is a programming agent for cardiovascular disease. *Placenta* **31** (suppl.), S54–S59 (2010).
40. J. Wang et al., Proteomic analysis and functional characterization of P4-ATPase phospholipid flippases from murine tissues. *Sci. Rep.* **8**, 10795 (2018).
41. H. Takatsu et al., ATP9B, a P4-ATPase (a putative aminophospholipid translocase), localizes to the trans-Golgi network in a CDC50 protein-independent manner. *J. Biol. Chem.* **286**, 38159–38167 (2011).
42. H. Katsuragawa et al., Monoclonal antiphosphatidylserine antibody reactivity against human first-trimester placental trophoblasts. *Am. J. Obstet. Gynecol.* **172**, 1592–1597 (1995).
43. M. Das et al., Phosphatidylserine efflux and intercellular fusion in a BeWo model of human villous cytotrophoblast. *Placenta* **25**, 396–407 (2004).
44. P. Žigon et al., Anti-phosphatidylserine/prothrombin antibodies are associated with adverse pregnancy outcomes. *J. Immunol. Res.* **2015**, 975704 (2015).
45. J. M. Whitlock, L. V. Chernomordik, Flagging fusion: Phosphatidylserine signaling in cell-cell fusion. *J. Biol. Chem.* **296**, 100411 (2021).
46. N. G. Brukman, B. Uygur, B. Podbilewicz, L. V. Chernomordik, How cells fuse. *J. Cell Biol.* **218**, 1436–1451 (2019).
47. Y. Zhang et al., TMEM16F phospholipid scramblase mediates trophoblast fusion and placental development. *Sci. Adv.* **6**, eaba0310 (2020).

48. H. Yang *et al.*, TMEM16F forms a Ca<sup>2+</sup>-activated cation channel required for lipid scrambling in platelets during blood coagulation. *Cell* **151**, 111–122 (2012).
49. T. Yeung *et al.*, Membrane phosphatidylserine regulates surface charge and protein localization. *Science* **319**, 210–213 (2008).
50. S. A. Degrelle, P. Gerbaud, L. Leconte, F. Ferreira, G. Pidoux, Annexin-A5 organized in 2D-network at the plasmalemma eases human trophoblast fusion. *Sci. Rep.* **7**, 42173 (2017).
51. C. A. Viall, L. W. Chamley, Histopathology in the placentae of women with antiphospholipid antibodies: A systematic review of the literature. *Autoimmun. Rev.* **14**, 446–471 (2015).
52. M. Tsuchiya *et al.*, Cell surface flip-flop of phosphatidylserine is critical for PIEZO1-mediated myotube formation. *Nat. Commun.* **9**, 2049 (2018).
53. M. Grifell-Junyent *et al.*, CDC50A is required for aminophospholipid transport and cell fusion in mouse C2C12 myoblasts. *J. Cell Sci.* **135**, jcs258649 (2022).
54. S. Nagata, Apoptosis and clearance of apoptotic cells. *Annu. Rev. Immunol.* **36**, 489–517 (2018).
55. G. W. Heyne *et al.*, A simple and reliable method for early pregnancy detection in inbred mice. *J. Am. Assoc. Lab. Anim. Sci.* **54**, 368–371 (2015).
56. K. Tokuhira, M. Ikawa, A. M. Benham, M. Okabe, Protein disulfide isomerase homolog PDILT is required for quality control of sperm membrane protein ADAM3 and male fertility [corrected]. *Proc. Natl. Acad. Sci. U.S.A.* **109**, 3850–3855 (2012).
57. L. S. Rodgers, D. C. Schnurr, D. Broka, T. D. Camenisch, An improved protocol for the isolation and cultivation of embryonic mouse myocytes. *Cytotechnology* **59**, 93–102 (2009).
58. N. Tabata *et al.*, Establishment of monoclonal anti-retroviral gp70 autoantibodies from MRL/lpr lupus mice and induction of glomerular gp70 deposition and pathology by transfer into non-autoimmune mice. *J. Virol.* **74**, 4116–4126 (2000).
59. S. Ray, B. Diamond, Generation of a fusion partner to sample the repertoire of splenic B cells destined for apoptosis. *Proc. Natl. Acad. Sci. U.S.A.* **91**, 5548–5551 (1994).
60. P. Chomczynski, N. Sacchi, Single-step method of RNA isolation by acid guanidinium thiocyanate-phenol-chloroform extraction. *Anal. Biochem.* **162**, 156–159 (1987).